Biophysical Journal Volume 104 April 2013 1495–1507

Proline Facilitates Membrane Insertion of the Antimicrobial Peptide Maculatin 1.1 via Surface Indentation and Subsequent Lipid Disordering

David I. Fernandez,[†] Tzong-Hsien Lee,[‡] Marc-Antoine Sani,[†] Marie-Isabel Aguilar,[‡*] and Frances Separovic[†*]
[†]School of Chemistry, Bio21 Institute, University of Melbourne, Victoria, Australia; and [‡]Department of Biochemistry and Molecular Biology, Monash University, Clayton, Victoria, Australia

ABSTRACT The role of proline in the disruption of membrane bilayer structure upon antimicrobial peptide (AMP) binding was studied. Specifically, ^{31}P and ^{2}H solid-state NMR and dual polarization interferometry (DPI) were used to analyze the membrane interactions of three AMPs: maculatin 1.1 and two analogs in which Pro-15 is replaced by Gly and Ala. For NMR, deuterated dimyristoylphosphatidylcholine (d_{54}-DMPC) and d_{54}-DMPC/dimyristoylphosphatidylglycerol (DMPG) were used to mimic eukaryotic and prokaryotic membranes, respectively. In fluid-phase DMPC bilayer systems, the peptides interacted primarily with the bilayer surface, with the native peptide having the strongest interaction. In the mixed DMPC/DMPG bilayers, maculatin 1.1 induced DMPG phase separation, whereas the analogs promoted the formation of isotropic and lipid-enriched phases with an enhanced effect relative to the neutral DMPC bilayers. In gel-phase DMPC vesicles, the native peptide disrupted the bilayer via a surface mechanism, and the effect of the analogs was similar to that observed in the fluid phase. Real-time changes in bilayer order were examined via DPI, with changes in bilayer birefringence analyzed as a function of the peptide mass bound to the bilayer. Although all three peptides decreased the bilayer order as a function of bound concentration, maculatin 1.1 caused the largest change in bilayer structure. The NMR data indicate that maculatin 1.1 binds predominantly at the surface regions of the bilayer, and both NMR and DPI results indicate that this binding leads to a drop in bilayer order. Overall, the results demonstrate that the proline at residue 15 plays a central role in the membrane interaction of maculatin 1.1 by inducing a significant change in membrane order and affecting the ability of the bilayer to recover from structural changes induced by the binding and insertion of the peptide.

INTRODUCTION

Studies examining the mechanism of antimicrobial peptide (AMP) action seek to define the structure of the final membrane disruption entity. Although this provides very important information in terms of the mechanism of disruption, there is still limited capacity to rationalize differences in the activity of closely related peptides. To provide a more detailed description of membrane binding and disruption, more specific information is required regarding the molecular changes that occur in the membrane bilayer from the point of first interaction to the final dissociation from, or disruption of, the membrane. This process includes multiple steps associated with changes in the peptide and membrane structure and the insertion/reorientation of the peptide, and characterization of these steps would clearly allow a more detailed definition of peptide-membrane interactions.

Maculatin 1.1 (GLFGVLAKVAAHVVPAIAEHF-NH_2) is a cationic AMP that is isolated from the skin secretions of the frog species *Litoria genimaculata* (1) and possesses antibacterial (1–6), antitumour (7), and antiviral (8) activity. Studies have shown that maculatin 1.1 interacts with model membranes composed of zwitterionic dimyristoylphosphatidylcholine (DMPC) and mixed DMPC/dimyristoylphosphatidylglycerol (DMPG) bilayers, with a greater effect on anionic membranes (5,9–12). Replacement of the Pro-15 residue results in a rearrangement into a tighter, more canonical α-helix with altered hydrophobicity and antimicrobial activity (13). These and other studies conducted on related families (2) indicate that maculatin 1.1 may exert its mode of action through a pore-formation mechanism (3,10,14–16).

As the peptide binds and reorients either partially or fully into the membrane interior, the phospholipid molecules also undergo a structural reorganization, and these changes in bilayer structure are integral to the process. Because biological membranes vary in composition among species, model membranes are used to define specific properties, such as the charge characteristics, of eukaryotic and prokaryotic membranes. Phosphatidylcholine lipids are common within eukaryotic organisms (17,18), whereas, despite variations among species, bacterial membranes tend to contain lipids with anionic headgroups that are effectively mimicked by the use of phosphatidylglycerol. For many systems, the specific lipid phase chosen also modulates peptide-membrane interactions. Previous AMP studies typically used fluid-phase (L_α) lipid membranes, but certain AMPs, such as magainin 2 and the membrane-lytic peptide melittin, have been shown to have enhanced interactions with gel-phase lipid systems (19–25). Similarly, quartz crystal microbalance-dissipation (16) and dual polarization interferometry (DPI) (26) studies of several frog AMPs,

Submitted December 6, 2012, and accepted for publication January 28, 2013.

*Correspondence: fs@unimelb.edu.au or mibel.aguilar@monash.edu

Editor: Mei Hong.

0006-3495/13/04/1495/13 $2.00
http://dx.doi.org/10.1016/j.bpj.2013.01.059

including aurein 1.2 and maculatin 1.1 (16,26), showed stronger interactions in supported lipid bilayers (SLBs) below the gel-fluid transition temperature.

A feature of many AMPs is the presence of a proline residue, which has a significant effect on the peptide structure and biological activity. However, how the proline residue exerts its effect on biological activity in terms of membrane structure is not clear. Solid-state NMR is a powerful tool for studying the effect of peptides on phospholipid bilayer structure and characterizing the membrane-binding properties of a range of peptides (5,13,15,19,24,27–32). Recently, we described the application of DPI to the analysis of membrane bilayer structure in terms of changes in birefringence (26,33–35), which provided apparently new insight into molecular events throughout the peptide-binding process. In the study presented here, we used solid-state NMR and DPI to analyze the effects of proline substitution in the AMP maculatin 1.1 on the bilayer structure of neutral and net anionic phospholipid membranes. Proline has a specific effect on peptide and protein structure and flexibility (29,36–41), and the changes in membrane structure induced by the binding of these peptides reveal the critical role of the proline residue in the disruption of the bilayer structure.

MATERIALS AND METHODS

Preparation of NMR samples

Perdeuterated-acyl chain 1,2-dimyristoyl-*sn*-glycero-3-phosphocholine (d_{54}-DMPC) and natural abundance 1,2-dimyristoyl-*sn*-glycero-3-[phospho-*rac*-(1-glycerol)] (DMPG) were purchased from Avanti Polar Lipids (Alabaster, AL) and used without further purification. Maculatin 1.1, maculatin P15G, and maculatin P15A were obtained from Mimotopes (Melbourne, Australia) with a purity of >90%. HCl solution was added before each peptide was lyophilized (42) to ensure that any traces of trifluoroacetic acid were removed.

Lipid films were prepared from d_{54}-DMPC or d_{54}-DMPC/DMPG (2:1 molar ratio) dissolved in $CHCl_3$/MeOH. Dried lipid thin films typically were hydrated with 500 μL of Milli-Q water before being lyophilized. The dried samples typically were rehydrated with 100 μL of 10 mM MOPS (3-(N-morpholino) propanesulfonic acid) buffer (pH 7) or peptide solubilized in MOPS buffer to a 10:1 lipid/peptide (L/P) molar ratio and subjected to five cycles of freeze-thaw before being transferred into NMR rotors or 5 mm NMR glass sample tubes. Typically 1 mg of peptide and 4 mg of phospholipid were used.

Solid-state NMR experiments

Static deuterium spectra were obtained at 46.1 MHz on a Varian Inova-300 spectrometer (Palo Alto, CA) using a composite-pulse solid-echo sequence. Operating conditions included 4.1 μs 90° pulses, 40 μs echo delay, and 0.5 s recycle time. Typically a minimum of 20,000 scans were collected and Fourier transformed using zero-filling to 16,384 points with 200 Hz exponential line-broadening. Oriented spectra were generated by dePaking in the time domain using a recently developed nmrPipe macro (Dr. John Gehman, University of Melbourne). The dePaked spectrum was fit with Gaussian line shapes and converted to order parameters by dividing the static splitting of each 26 myristoyl CD_n position with a static coupling constant of 255 kHz (43).

^{31}P static solid-state NMR experiments were performed at 121.5 MHz on a Varian Inova-300 spectrometer using a Hahn echo pulse sequence with proton decoupling. Typically a 4.4 μs 90° pulse was used with 29 μs echo time and 3 s recycle delay. A minimum of 20,000 scans were collected and processed with 100 Hz exponential line-broadening and zero-filling to 8,192 points. Static ^{31}P NMR spectra were deconvoluted as previously described (13).

Each sample was subjected to a temperature cycle in which the static deuterium and phosphorus spectra were acquired with the bearing air supply set first to 30°C, 20°C, and 15°C, and then reheated to 30°C. The NMR probe was removed from the magnetic field between each temperature change and the samples were allowed to equilibrate for a minimum of 1 h and then replaced in the magnet for 15–20 min before spectra were collected.

Liposome preparation for DPI

Thin lipid films of DMPC and DMPC/DMPG (4:1) were hydrated to 1 mM lipid concentration with 10 mM MOPS, 150 mM NaCl pH 7.0, buffer solution at 37°C for 1 h with constant vortexing. The hydrated lipid suspension was sonicated in a water bath for ~30 min at 37°C and extruded before use through 50 nm polycarbonate membranes (19 times) using an Avestin Liposfast extruder (Ottawa, Canada).

Deposition of SLBs on sensor chips

Planar SLBs were prepared via in situ adsorption of liposomes to a silicon oxynitride waveguide sensor chip. An unmodified FB80 AnaChip (Farfield Group, Manchester, UK) was clamped inside a dual-zone temperature-controlled housing. The temperature was controlled to within 0.005°C using a Peltier system. A 100-μm-thick fluorosilicon gasket containing two separate 1.7 μL microfluidic channels was clamped over the sensing waveguide. FB80 waveguide chips were cleaned and calibrated for their optical properties as previously described (26,35). The bulk buffer solution (10 mM MOPS, 150 mM NaCl, pH 7.0) was used as the flow media throughout all experimental steps, and all solutions were degassed before use. Flow rate during experiments was controlled with the use of a Harvard Apparatus PHD2000 programmable syringe pump. For lipid bilayer formation, the temperature of the system was set to 28°C. The previously prepared lipid stock suspension then was extruded and diluted to 0.1 mg/mL with further MOPS buffer containing 1 mM $CaCl_2$, which was added to promote vesicle rupture and SLB formation (44–46).

The liposome solutions were injected for 10 min at a flow rate of 20 μL/min, and immediately afterward, further bulk buffer with 1 mM $CaCl_2$ was injected (200 μL at 20 μL/min) to stabilize the SLB. The adsorbed bilayer was then allowed to equilibrate for 20 min under running buffer until a stable baseline had been achieved. The temperature was then set to either 20°C or 30°C depending on the experiment and allowed to equilibrate before peptide addition.

Maculatin 1.1, maculatin P15A, and maculatin P15G were prepared at concentrations of 1, 2, 5, 10 and 20 μM in the running buffer (10 mM MOPS, 150 mM NaCl, pH 7.0). A fresh bilayer was used for each individual peptide measurement and 160 μL of each concentration was injected sequentially onto the SLB in increasing concentrations at a flow rate of 40 μL/min, with a total of 30 min equilibration time between injections.

DPI

Data acquisition was carried out using AnaLight200 version 2.1.0 software and analyzed using AnaLight Explorer proprietary software as previously described (26,35,47). The theory of DPI has been treated more extensively in previous papers (26,35,47–50) and a basic description is provided in the Supporting Material.

RESULTS

Peptide-lipid acyl chain interaction observed by ^{2}H static solid-state NMR

^{2}H NMR analysis of acyl chain deuterated phospholipid bilayers provides information about the acyl chain order and interactions occurring within the membrane (51). ^{2}H NMR experiments were performed to determine the effects of the maculatin analogs on the acyl chains and bilayer structure below and above the gel- to fluid-phase transition temperature.

DMPC (Fig. 1 *a*) and DMPC/DMPG bilayers gave typical order parameter profiles (13), and inclusion of DMPG had little effect on the DMPC acyl chain order (Figs. 1 *b* and 2) (13,31). The order parameters of DMPC (Fig. 1 *a*) with maculatin 1.1 and P15G were reduced by ~19% and ~5%, respectively, whereas minimal change was seen with P15A. A 5–10% decrease in lower acyl chain order was seen in d_{54}-DMPC/DMPG bilayers with maculatin 1.1 and P15A, whereas P15G had a more complex effect and the spectra contained features of a mixed gel/fluid phase (Figs. 1 *b* and 2).

At 20°C, which is just below the gel-fluid transition of the pure lipids, the spectra were characteristic of immobilized $L_{\beta'}$ gel-phase lipids. Gel-phase spectra were observed for maculatin 1.1 and P15A with DMPC (Fig. 2), with a small isotropic peak for maculatin 1.1. Fluid-phase characteristics with moderate broadening were observed with maculatin P15G in DMPC. A similar spectrum was observed for the anionic bilayer with maculatin 1.1, whereas mixed lipid phases were observed with both maculatin analogs.

At 15°C, gel-phase spectra were observed for the lipid-only samples. Maculatin 1.1 produced a broad isotropic ^{2}H spectrum in DMPC, whereas both analogs produced mixed gel- and isotropic-phase spectra in both types of lipid bilayers.

Heating through the gel- to fluid-phase transition back to 30°C (Fig. 1, *c* and *d*) resulted in fluid lamellar phases with reduced order and resolution for DMPC bilayers with maculatin 1.1 and P15G. By contrast, acyl chain order increased with P15A. In DMPC/DMPG, order uniformly decreased slightly with maculatin 1.1 (Fig. 1 *d*). With P15G, we detected a mixed gel/disordered fluid phase similar to that observed before the decrease in temperature, suggesting that the peptide stabilized lipid domains in the bilayer. For P15A, the order parameters decreased ~10% in the upper acyl chain regions and 1–2% in the lower regions. Thus, a slow passage through the gel-fluid transition, as opposed to the rapid freeze/thaw steps performed during sample preparation, led to a greater effect of the peptide on the lipid bilayer.

Probing phospholipid headgroup dynamics by static ^{31}P solid-state NMR

^{31}P NMR of phospholipid bilayers gives information on the lipid phase, local order, and dynamics within the phosphate region of the lipid (52). Fluid lamellar (L_α) phospholipid liposomes produce an axially symmetric powder pattern (chemical shift anisotropy (CSA)) whose overall width depends on headgroup orientation and disorder (53). Hence, ^{31}P NMR was used to probe peptide-induced headgroup

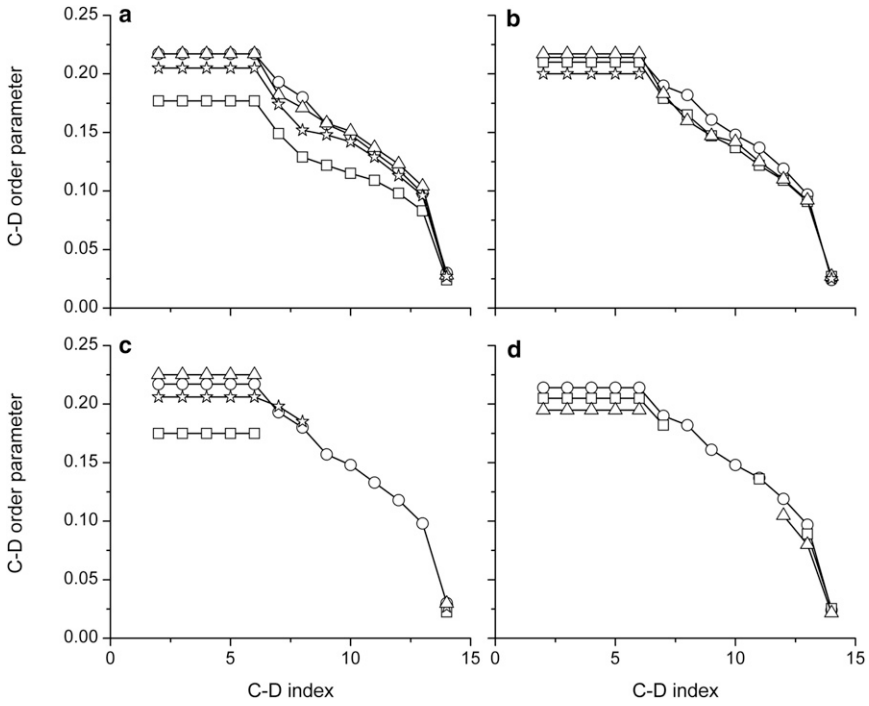

FIGURE 1 Order parameter profile obtained from dePaked spectra of maculatin 1.1 and analogs in d_{54}-DMPC (*left*) and d_{54}-DMPC/DMPG (2:1) (*right*) at 30°C (*top*) and after temperature cycling through 15°C and a return to 30°C (*bottom*). Lipid alone (*circles*), lipid + maculatin 1.1 (*squares*), lipid + P15G (*stars*), and lipid + P15A (*triangles*).

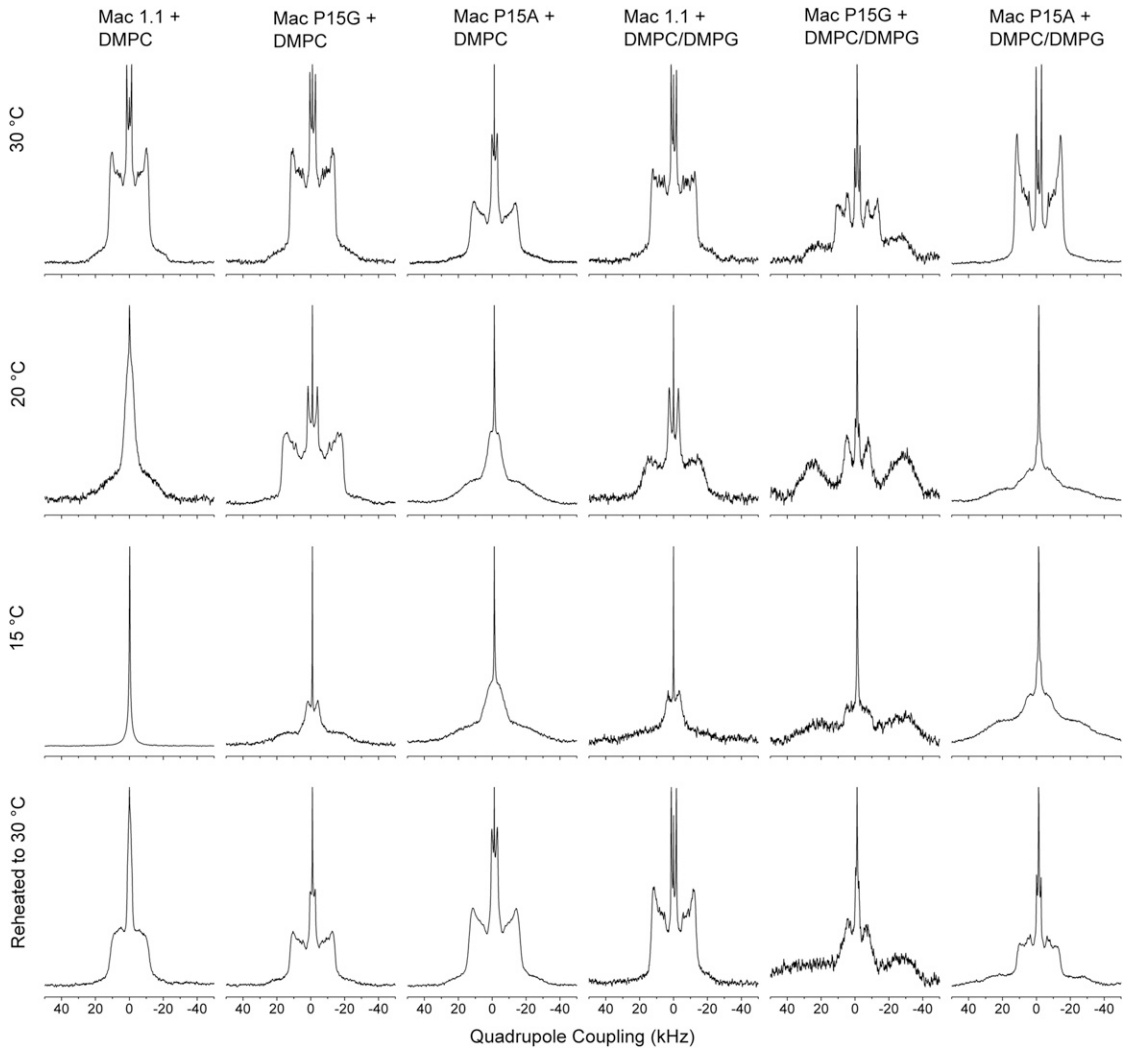

FIGURE 2 ^{2}H NMR spectra of d_{54}-DMPC (*left*) and d_{54}-DMPC/DMPG (2:1) (*right*) phospholipid bilayers with maculatin 1.1, maculatin P15G, and maculatin P15A. Spectra were recorded at 30°C, 20°C, and 15°C, and reheated to 30°C.

perturbations. Multilamellar vesicles produced typical powder patterns at 30°C, with a CSA of ~45 ppm for DMPC and overlapping 40 and 31 ppm CSA for DMPC and DMPG, respectively, in the mixed lipid bilayer (not shown). Maculatin 1.1 and P15A reduced the DMPC CSA by 33% and 23%, respectively, whereas P15G had less effect (−9%; Fig. 3 and Table 1). In the mixed bilayer, the peptides produced two clearly distinguishable CSAs, but both analogs also led to broad isotropic signals (Fig. 3).

When cooled below its gel-fluid transition to 20°C (54), DMPC (and DMPC/DMPG) formed a mixed ordered and disordered $P_{\beta'}$ ripple phase (55,56). With maculatin 1.1, the CSA was further reduced and a larger isotropic peak indicated additional disorder. No large changes were observed with P15G, and P15A gave only a minor CSA increase with a small isotropic signal. No major change in DPMC/DMPG was seen with maculatin 1.1, but both analogs showed a greater effect than on the neutral bilayer. The isotropic signal and CSA linewidth increased with P15A, and an additional broad CSA formed with P15G.

No significant spectral change occurred for DMPC at 15°C. With maculatin 1.1, a fully isotropic spectrum formed (Fig. 3), indicating a very significant bilayer disruption. Formation of an immobilized lipid phase was observed with P15A, whereas disorder increased for P15G with a reduction in CSA and formation of a small isotropic peak. In the anionic DMPC/DMPG system, maculatin 1.1 produced a small isotropic peak. With P15A the isotropic signal was reduced and an additional 50 ppm CSA was formed, whereas with P15G, both bilayer CSA components moderately broadened and the isotropic signal increased in proportion.

Returning to 30°C yielded similar spectra for the lipid-only spectra as observed previously, but for maculatin 1.1 with DMPC, a heavily disordered bilayer reformed. No significant change was seen with P15A or P15G, apart from a small fraction of signal showing an isotropic phase.

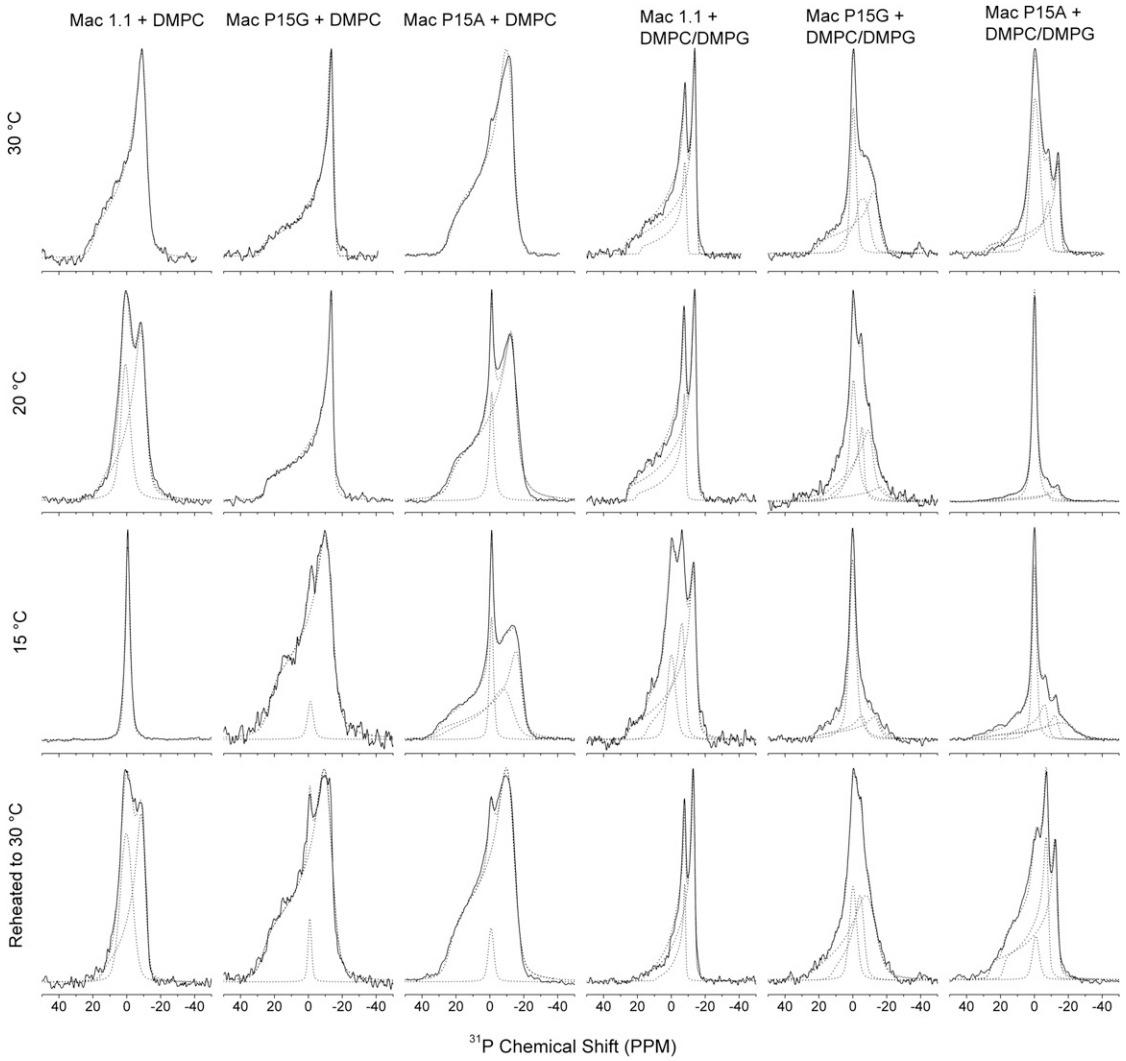

FIGURE 3 ^{31}P NMR spectra of DMPC (*left*) and DMPC/DMPG (2:1) (*right*) phospholipid bilayers with maculatin 1.1, P15G, and P15A. Spectra were recorded at 30°C, 20°C, and 15°C, and reheated to 30°C. Unbroken lines represent the experimental spectra. Dotted lines represent deconvoluted components.

In the mixed-lipid system, two clearly distinguished CSAs were observed with maculatin 1.1, but, as for DMPC, each bilayer CSA was narrower than it was initially. Maculatin P15A broadened the CSAs and altered the proportions relative to initial values, whereas the isotropic signal decreased. Maculatin P15G behaved similarly to maculatin 1.1: the major CSAs were narrower than their initial values and the isotropic signal decreased.

Overall, the NMR studies demonstrate that all three peptides alter the bilayer structure of both membrane systems and the bilayer disruption is significantly modulated by temperature.

Interaction of maculatin peptides with SLBs

We studied the membrane-binding characteristics of maculatin peptides and their effects on the membrane structure using DPI on consistent and well-defined supported phospholipid bilayers. The structural parameters of supported DMPC and DMPC/DMPG (4:1 molar ratio) bilayers formed via in situ liposome deposition and characterized by DPI are listed in Table 2. The mass, density, thickness, and birefringence values of each bilayer are consistent with a thinner, more disordered bilayer at 30°C and a thicker bilayer with a more orderly alignment of lipid molecules at 20°C. These values are also consistent with complete surface coverage by unilamellar bilayers and were highly reproducible for all binding assays.

The accumulative binding of each maculatin peptide at 1, 2, 5, 10, and 20 μM were characterized by the *transverse* magnetic (TM) and *transverse* electric (TE) phase changes obtained at both 30°C and 20°C for the fluid- and gel-state membranes, respectively. The L/P ratios were first determined for each peptide-bilayer system at the end of the

TABLE 1 Effect of maculatin 1.1 and analogs on ^{31}P NMR CSA of DMPC and DMPC/DMPG (2:1) multilamellar vesicles

	DMPC				DMPC/DMPG (2:1)			
Temp	Lipid bilayer	Mac1.1	Mac P15G	Mac P15A	Lipid bilayer	Mac1.1	Mac P15G	Mac P15A
30°C	45.5	30.4	41.6	35.2	40 (68) 31.2 (32)	41.8 (74) 26.5 (23)	43 (39.5) 27.5 (23) Iso (37.5)	34.9 (58) 24 (22) Iso (20)
20°C	56.3 (57) 40.4 (42) Iso (1)	26.5 (67) Iso (33)	40	37.4 (88.5) Iso (11.5)	41 (61.5) 27.5 (33.5) Iso (5)	39.8 (73.5) 28.9 (26.5)	47.3 (11) 27.5 (39) 19.6 (21) Iso (29)	40.1 (18) 25.8 (7.5) Iso (74.5)
15°C	56.4 (61) 40 (36.5) Iso (2.5)	Iso	35.4 (96) Iso (4)	49.1 (52) 38.4 (35.5) Iso (12.5)	47 (12) 42.5 (41.5) 16.2 (31) Iso (15.5)	39.1 (55.5) 22.1 (29.5) Iso (15)	36.3 (23) 27.9 (19) Iso (58)	49.6 (27.5) 41 (19) 22.7 (21) Iso (32.5)
Reheat to 30°C		24.5 (57) Iso (43)	38.6 (96) Iso (4)	35.8 (95) Iso (5)		29.5 (78) 17.2 (22)	34.1 (56.5) 17.8 (26) Iso (17.5)	39.1 (52) 25.9 (41) Iso (7)

Numbers in parentheses indicate % contribution to signal.
Iso, isotropic peak.

association phase and are listed in Table 2. The L/P values range from 4:1 to 35:1 and reflect the variation in the amount of peptide bound. These values also correlate with the 1:10 L/P ratio used to prepare the samples for NMR analysis, and confirm that the DPI experiments were performed within a similar ratio.

TM and TE phase changes for each peptide binding to DMPC and DMPC/DMPG (4:1) are shown in Fig. 4. Small increases in TM and TE phase changes were observed at low concentrations (<5 μM) for all three peptides binding to the DMPC SLB, with different behavior at higher concentrations (5–20 μM). Maculatin 1.1 caused large TM and TE phase changes above 5 μM at 30°C and 20°C. Maculatin P15G only showed a large phase change at 20 μM at 30°C and above 5 μM at 20°C, and a higher peptide concentration was required for binding to the more-fluid SLB (30°C) compared with maculatin 1.1. Similarly, large irreversible TM and TE phase changes were observed for the binding of 10 μM P15A to the more-fluid DMPC (30°C) or for binding of 5 μM P15A to the gel-like DMPC (20°C). Although a higher peptide concentration was required to generate large increases in the TM and TE phases, the effects were larger than those observed for maculatin 1.1. With both analogs, larger phase changes were observed in the more-ordered DMPC at 20°C.

The effect of peptide binding on a negatively charged membrane was also investigated. The molar fraction of DMPG was reduced to 20% for the DPI analysis, which

TABLE 2 DPI structural values and lipid/peptide ratios (L/P) for maculatin peptides binding to supported DMPC and DMPC/DMPG (4:1) lipid bilayers

	DPI structural values for SLBs				
	Density (g/cm^3)	Thickness (Å)	Mass (ng/mm^2)	Birefringence	Area/lipid (Å^2)
30°C					
DMPC	1.003 ± 0.003	45.1 ± 0.6	4.52 ± 0.06	0.0193 ± 0.0007	49.9 ± 0.7
PC/PG	1.007 ± 0.003	44.5 ± 1.0	4.48 ± 0.11	0.0200 ± 0.0009	50.5 ± 1.2
20°C					
DMPC	1.002 ± 0.002	47.2 ± 0.8	4.73 ± 0.08	0.0223 ± 0.0003	47.6 ± 0.82
PC/PG	1.004 ± 0.004	47.5 ± 1.2	4.77 ± 0.1	0.0223 ± 0.0003	47.4 ± 1.0

Peptide	Concentration (μM)	L/P			
		30°C		20°C	
		DMPC	PC/PG (4:1)	DMPC	PC/PG (4:1)
Mac 1.1	5	9.4	24.1	10.6	9.6
	10	7.3	11.3	9.1	9.4
	20	6.6	11	8	9
Mac P15G	5	36	16.6	13.2	13.5
	10	20.8	6.6	6.5	5.6
	20	5.9	6	5.8	4.6
Mac P15A	5	35.5	51	16.3	12.2
	10	5.8	20.6	5.5	5.4
	20	4.1	5.4	4	4

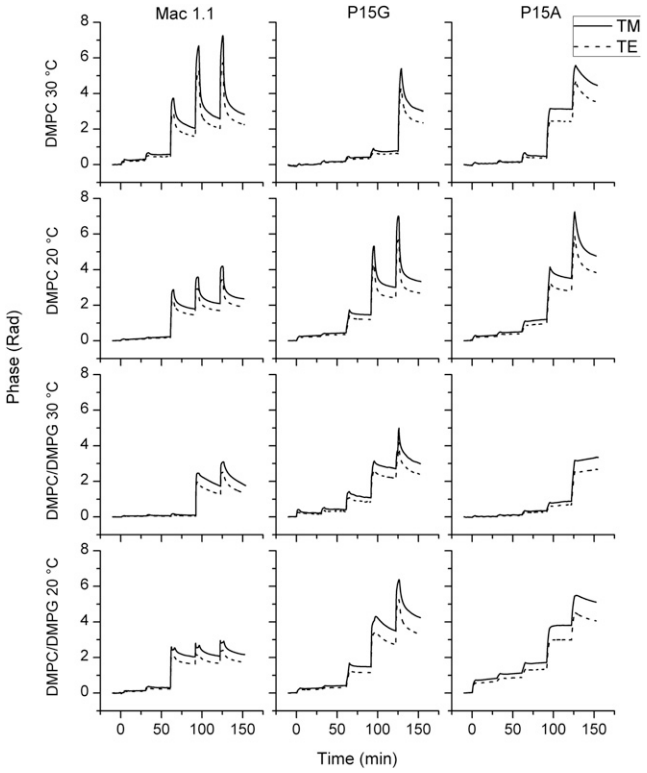

FIGURE 4 Real-time TM and TE phase changes in radians for consecutive injections of 1, 2, 5, 10, and 20 μM maculatin 1.1, P15G, and P15A onto planar solid supported DMPC and DMPC/DMPG (4:1) bilayers at 30°C and 20°C.

resulted in consistent formation of well-defined bilayers while retaining a suitably anionic surface. Similarly to the DMPC SLB, all three peptides showed little to no binding below 5 μM, except for P15A at 20°C. Above 10 μM, maculatin 1.1 induced significant phase changes at 30°C but they were of a lower magnitude than observed with the DMPC SLB. At 20°C, large phase changes occurred above 5 μM and there was less dissociation than at 30°C. At 5 μM and above, P15G induced large TM and TE phase changes (with a greater change at 20°C) that were larger than the phase changes caused by maculatin 1.1. By contrast, maculatin P15A bound irreversibly above 5 μM, with small and large phase changes seen at 30°C and 20°C, respectively.

The measured TM and TE phases were subsequently resolved into the mass of membrane-bound peptide and birefringence for both lipid bilayers. Plots of mass changes versus time and birefringence versus time are shown in Figs. S1 and S2. However, because both the peptide mass and the structural changes associated with their binding to the lipid bilayer contribute to the measured TM and TE phase changes, analysis of changes in bilayer order as a function of peptide mass allows the impact of peptide binding on the membrane structure to be analyzed. The changes in DMPC and DMPC/DMPG bilayer order induced by maculatin 1.1 and both analogs are shown in Fig. 5, with the association phase indicated by the solid arrow and dissociation indicated by the dotted arrow.

The binding of maculatin 1.1 to the more-fluid DMPC showed a small decrease in birefringence at low peptide mass. As maculatin 1.1 accumulated on the DMPC bilayer, birefringence did not initially change, but it then decreased as the membrane-bound maculatin 1.1 reached a threshold value, as indicated by the inflection points in Fig. 5. In comparison, P15G induced a small disordering in the more-fluid DMPC initially with a greater level of disordering observed at high peptide mass. Such disordering was almost reversible after the peptide dissociated from the membrane, which resulted in a very small degree of overall disordering in the more-fluid DMPC SLB. The binding of P15A to DMPC at 30°C induced the largest disordering with the highest amount of bound peptide. This disordering was irreversible at lower concentrations and only became partially reversible at high peptide mass.

At 20°C, in contrast, the binding of maculatin 1.1 and both analogs to DMPC caused a linear decrease in bilayer order, even at very low amounts of bound maculatin 1.1. With the subsequent addition of peptide to the DMPC bilayer, maculatin 1.1 induced more disorder at 20°C than in the more-fluid DMPC at 30°C. The changes in the bilayer order were irreversible up to a certain amount of peptide bound to the membrane or a critical L/P ratio, which showed as inflection points in the birefringence versus mass plot. The changes in the bilayer order then became a reversible process when more peptide bound beyond this critical L/P ratio. Maculatin P15G also induced a large linear decrease in bilayer order, but the change in birefringence of DMPC at 20°C was greater than that observed for maculatin 1.1. This reversible disordering indicated that the more-fluid bilayer at 30°C recovered to the initial membrane ordering more effectively than the lower-temperature phase. Thus, the substitution of proline to glycine resulted in more bound peptide and exerted a larger impact on DMPC order at 20°C than on the more-fluid DMPC at 30°C. The P15A analog showed the highest amount of binding and also induced the largest disordering in DMPC at 20°C, which only became partially reversible at 20 μM.

The changes in the molecular order of the DMPC/DMPG bilayers induced by the binding of maculatin peptides at 30°C and 20°C are shown in Fig. 5 and show distinct differences compared with DMPC. The binding of maculatin 1.1 to the more-fluid DMPC/DMPG SLB at 30°C resulted in small increases in bilayer order at low levels of membrane-bound peptide. Significant bilayer disorder was observed with subsequent increases in the mass of maculatin 1.1 bound to DMPC/DMPG. High levels of P15G bound to the more-fluid DMPC/DMPG, which was associated with the induction of large decreases in bilayer order that were only partially reversible during the peptide dissociation. Maculatin P15A bound to the

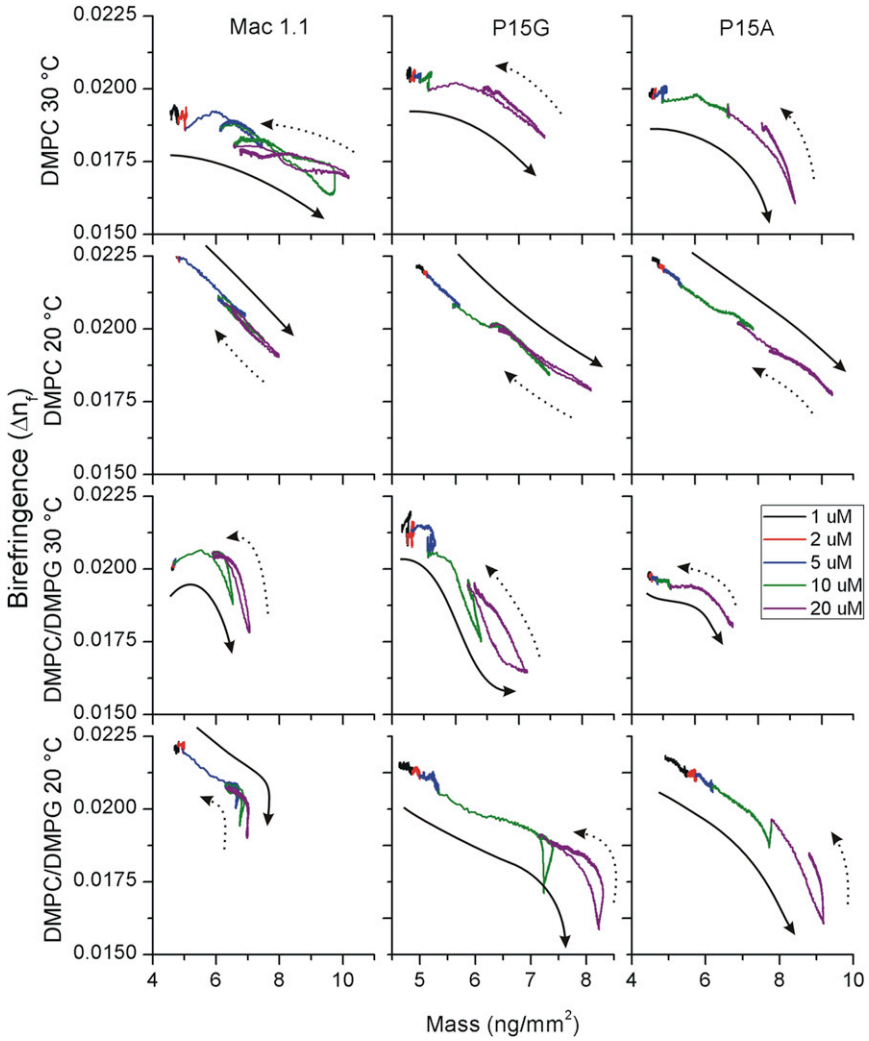

FIGURE 5 Birefringence (molecular order) changes in supported DMPC and DMPC/DMPG (4:1) lipid bilayers as a function of mass of membrane bound peptide at 30°C and 20°C. Changes were calculated for consecutive injections of 1, 2, 5, 10, and 20 μM maculatin 1.1, P15G, and P15A. Arrowed lines indicate association (*solid line*) and dissociation (*dotted line*) phases.

more-fluid DMPC/DMPG with the largest amount and induced a relatively greater decrease in bilayer order than maculatin 1.1 and P15G.

At 20°C, the bilayer order of DMPC/DMPG decreased at low levels of bound maculatin 1.1 and showed a large and sharp decrease in bilayer order when maculatin 1.1 reached a critical amount. This large, sudden disordering was not observed with the neutral DMPC membranes. The changes in DMPC/DMPG order at 20°C induced by P15G also showed a large sharp decrease in bilayer order similar to that observed for maculatin 1.1. However, more P15G was bound and induced more disordering in the DMPC/DMPG SLB than maculatin 1.1. Maculatin P15A gradually accumulated on DMPC/DMPG and resulted in the largest amount of peptide bound. The disordering of the DMPC/DMPG SLB induced by P15A was similar to that induced by P15G and larger than that induced by maculatin 1.1. These overall differences show that the negative charges on the membrane surface resulted in a greater susceptibility of the bilayer to peptide-induced disordering.

DISCUSSION

The disruption of a phospholipid bilayer by AMPs is associated with a complex series of geometrical and dynamic changes that occur within the lipid matrix during peptide association-dissociation, insertion, and, ultimately, disruption of membrane integrity. Maculatin 1.1 has been shown to have significant effects on the membrane bilayer structure. We propose that the proline residue at position 15 plays a critical role in the activity of maculatin 1.1 by facilitating the disruption of the membrane bilayer structure. Thus, to unravel the mechanism of action, it is crucial to characterize the effects on the membrane structure throughout the process of peptide binding leading to insertion. In this study, we used NMR and DPI to investigate the effect of proline substitution on the characteristics of maculatin 1.1 binding to lipid bilayers composed of DMPC and DMPC/DMPG. Specifically, the effects of replacing Pro-15 with Gly and Ala in maculatin 1.1 on the membrane structure were investigated. To obtain further insight into peptide selectivity and insertion mechanisms in terms of changes in membrane

structure and order, we also investigated the role of negatively charged phospholipids and lipid phases, such as the ordered/disordered $P_{\beta'}$ ripple phase (21,25), in modulating the membrane-destabilization effects of the maculatin analogs.

The NMR studies showed evidence of different membrane structures in the presence of each peptide. In particular, the isotropic phase was quite prevalent under some conditions and is consistent with the formation of a toroidal pore-like network. The ability of each peptide to induce this structure, together with the capacity of the membrane to recover, either through temperature changes or after peptide dissociation, provides (to our knowledge) new information that allows us to establish a more-detailed mechanistic understanding of AMP action.

The large reductions in ^{31}P CSA (Table 1) and ^{2}H order parameter profiles of the lipid bilayers (Fig. 1) are an indication of increased disorder promoted by peptide interaction. The reduction in the acyl chain order and CSA linewidth suggests that these peptides perturb DMPC bilayers, exhibiting a primarily surface interaction with fluid-phase DMPC bilayers. The formation of visually distinct CSA and isotropic signals, together with the coexistence of mixed lipid phases in the anionic bilayers, indicates that these peptides actively perturb the bilayer and may segregate lipids and promote demixing or domain formation (57,58). The extent of bilayer disordering as indicated by the NMR data followed the order Mac P15G $<$ Mac P15A $<$ Mac1.1 and is consistent with the intercalation of each peptide between the lipid headgroups, which increased the disorder and motional freedom in both headgroup and acyl chains.

We investigated the effect of peptide binding on the bilayer structure throughout the gel- to fluid-phase transition by performing NMR measurements at 30°C, 20°C, and 15°C, and reheating to 30°C. Defects formed in the mixed ordered/disordered $P_{\beta'}$ ripple phase when each lipid system was taken below the gel-fluid transition. At 20°C, the effect of the peptide on the bilayer was moderately enhanced and manifested by the presence of a mixture of fluid, gel, and isotropic phases that likely were due to a broadening of the lipid phase transition, as previously seen with related peptides (9). A further reduction in temperature led to complete destabilization of the DMPC bilayer by the native peptide. The complete absence of a bilayer CSA and formation of isotropic ^{31}P and ^{2}H NMR spectra indicates that small, rapidly tumbling lipid aggregates were formed in a manner similar to that reported for magainin (19,20) and reminiscent of the carpet model described by Shai (59,60). Maculatin P15G and P15A had a less dramatic effect, with the spectra affected by slower lipid motions due to the reduced temperature. For the mixed DMPC/DMPG lipid bilayers, additional disorder was seen in the form of small isotropic peaks with both maculatin 1.1 and P15G, together with a general reduction in motions for the bilayer phase for all three peptides. Although the membrane integrity was significantly restored after this temperature transition, the native peptide significantly perturbed the bilayer and a larger isotropic component remained than was seen with either of the two analogs, which suggests that the proline residue causes a greater perturbance in the bilayer structure from which it cannot readily recover even when the temperature is restored to 30°C.

Similar effects were previously observed for melittin, which induces the formation of small 20- to 40-nm lipid discs in phospholipid bilayers after passing through the gel- to fluid-phase transition into the ripple and gel phase (21,25). A reversible transition between disc-like micelles and extended bilayers occurs with temperature through the DMPC phase transition (23) and is driven by peptide interaction with defects formed in the gel and intermediate ripple phases. Likewise, magainin 2 induces the formation of isotropic ^{31}P NMR signals in DMPC bilayers below the phase transition (19). In a similar manner, sphingomyelin and phosphatidylcholine bilayers were more effectively solubilized by detergent in the gel phase, reflecting a stronger interaction with the fluid phase (61). In this study, both analogs caused a small increase in the order of the acyl chain region nearer to the headgroup, with the P15A analog increasing order even at the terminal methyl of the acyl chain. This indicates that the absence of the proline residue promoted an increased bilayer order akin to that observed with melittin in phosphatidylcholine multilayers (32).

We also examined the effects of both fluid and gel-like phases on maculatin 1.1-induced membrane changes by DPI at 30°C and 20°C in terms of changes in the birefringence as a function of the mass of bound peptide. The results obtained at 30°C were also consistent with surface binding of each peptide to the fluid DMPC at lower concentrations. However, the overall birefringence-mass profile for maculatin 1.1 differed in shape compared with the profile for the two analogs. For maculatin 1.1, there were large reversible changes in birefringence at 5, 10, and 20 μM, which when considered together with the presence of a significant isotropic peak by NMR suggests that the decrease in birefringence corresponds to the formation of toroidal-type structures. Furthermore, this membrane structural change was partially reversible, as evidenced by both the NMR and DPI data. In contrast, the birefringence-mass profiles for both maculatin P15G and P15A were curvilinear and only partially reversible at the highest concentration. Thus, in the presence of these two analogs, the fluid phase of DMPC was initially more resistant to structural changes until a threshold peptide concentration was reached, followed by a sharp decline in membrane order, which only partially recovered after dissociation of the peptide. In contrast, the birefringence-mass profiles for all three peptides with DMPC at 20°C showed a linear decline reflecting a greater susceptibility of the more-rigid bilayer to peptide disruption. Moreover, there was a greater decrease

in birefringence (i.e., membrane order), and this drop in membrane order became more irreversible according to maculatin 1.1 < P15G < P15A.

Previous studies showed significant interactions between maculatin peptides and anionic model bilayers in the fluid phase that are consistent with lipid domain formation for the native peptide and the formation of highly disordered structures akin to toroidal pores with the analogs (5,9,11,13,15). In this study with mixed lipid bilayers, DMPG enabled greater freedom of motion in the headgroup region below the phase transition temperature compared with the DMPC-only system. Moreover, the ^{2}H spectrum was consistent with gel-phase lipid acyl chains for each of the peptides, indicating that the large ^{31}P NMR peaks centered about the isotropic chemical shifts were due to highly curved lipid structures more in keeping with a toroidal pore rather than formation of rapidly tumbling aggregates, as in the carpet model, which additionally would also partially average out the broader ^{2}H spectra. Further reduction in temperature led to additional disruption with an isotropic component enriched in DMPC for the native peptide, whereas the interaction with the maculatin P15G analog was significantly enhanced with a large isotropic component and no observable reduction in lipid motion at the low temperature. The maculatin P15A analog exhibited slower motions with a reduction in isotropic component, which was likely due to highly disordered lipid rather than small rapidly tumbling aggregates. In similarity to the DMPC systems, raising the temperature back above the phase transition allowed the lamellar bilayer to reform, although it was more perturbed relative to the starting condition, suggesting that temperature cycling enhanced the peptide interaction. The disordering of the DMPC/DMPG bilayer induced by the maculatin peptides also showed distinctive inflection points in the birefringence versus mass plot corresponding to large decreases in birefringence without significant changes in peptide mass. Similar inflection points were previously observed for the interaction of aurein with DMPC-containing membranes at a particular L/P threshold (26). However, in the case of aurein, the membrane structure changes corresponded to membrane lysis. By comparison, because we found no evidence of membrane lysis in this study, the inflection points for the maculatin peptides are likely to correspond to major membrane disordering, as evidenced by the isotropic peaks in the NMR spectra. Moreover, as observed for DMPC, the curves were similar for each peptide, but the inflection points occurred at increasingly higher bound peptide mass, indicating that although all three peptides act via a similar mechanism of bilayer disruption, different levels of peptide are required to exert their effect.

AMPs generally form amphipathic α-helices in membrane-like environments, which is essential for activity (2) and interaction with bacterial membranes. We recently demonstrated that maculatin 1.1, P15G, and P15A adopt a helical structure in DMPC and DMPC/DMPG bilayers (6). Replacing Pro in native maculatin with Ala (maculatin P15A) skews the solution structure into a tighter, more canonical α-helix that lacks the significant kink of the native peptide and reorients the distribution of residues such that the amphipathicity is altered (4,5,13) and an increase in hemolytic activity occurs (6). However, the Pro-to-Ala replacement resulted in a 5- to 10-fold decrease in antimicrobial activity (4). The ability of the peptide to change conformation at the Pro residue, as seen for melittin (29,32), the αM2 transmembrane segment of the nAChR (37), and other AMPs (41,62) in lipid bilayers, may facilitate insertion. The results presented here, therefore, strongly suggest that maculatin 1.1 is generally the most effective peptide of the three analogs due to its kinked structure, which can more easily perturb the bilayer structure than the linear helical structures of maculatin P15G and P15A. Moreover, the anionic bilayers are more susceptible to peptide effects than the zwitterionic bilayer, predominantly as a result of the lipid domains that form upon the binding and insertion of the peptides.

A similar effect of proline on membrane interactions has been observed for a number of peptides. For example, proline analogs of peptides derived from the *Helicobacter pylori* ribosomal protein L1 (HPA) were studied by surface plasmon resonance and DPI (35). The kink induced by proline was shown to disrupt the hydrophobic membrane binding and insertion face, which led to a lower amount binding to the membrane. The profiles of birefringence changes for maculatin peptides as a function of membrane-bound peptide mass more closely resembled the profiles obtained for the HPA peptides inserting into the bilayer. However, maculatin peptides induced a smaller degree of disordering as a function of peptide mass than the HPA peptides.

Model of maculatin membrane disruption

Based on these studies, we propose a model for the mechanism of action for maculatin-related peptides that centers on the effect of the kinked helical structure of maculatin 1.1. The NMR data indicate that maculatin 1.1 binds predominantly at the surface regions of the bilayer, whereas both the NMR and DPI results indicate that this binding causes a drop in the bilayer order. Maculatin 1.1 is strongly amphipathic along both ends of the helix, and to allow maximal interaction with the membrane surface, the peptide may cause the bilayer surface to indent to accommodate the kink and maximize the interaction with the entire peptide as shown schematically in Fig. 6. This surface imperfection/indentation then facilitates subsequent partial insertion of the peptide into the bilayer. According to the DPI and NMR results, this subsequent insertion was associated with a drop in the bilayer order after a certain level of bound peptide was achieved, although this drop in order was largely reversible in DMPC. The flexibility of the acyl chains plays an important role in the ability of the membrane to respond to

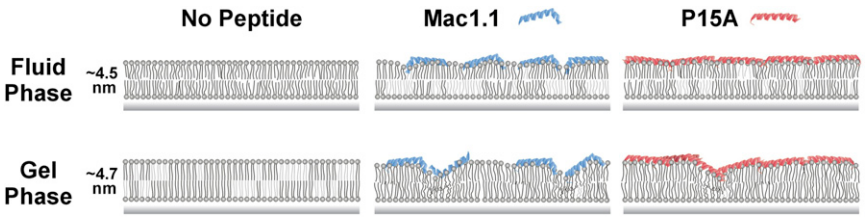

FIGURE 6 Schematic illustration depicting membrane bilayer structural changes upon the interaction of 20 μM maculatin 1.1 and P15A. Before peptide binding occurs, the gel phase is a thicker, more rigid bilayer. Upon peptide binding, changes in the lipid structure occur during initial peptide surface binding with minimal penetration of the bilayer interior. As the concentration increases, the initial surface binding is associated with partial insertion and disruption of membrane order facilitated by the kinked helical structure of maculatin 1.1. Subsequent steps involve partial insertion into the membrane, until an effective concentration of peptide accumulates followed by a rapid decrease in birefringence without further increase in mass, which indicates peptide organization on the surface before major bilayer disruption that may approximate a toroidal-like structure (63). Peptide dissociation and birefringence recovery follows, indicating removal of excess peptide and bilayer reordering to accommodate the inserted peptide. Overall, the threshold bound peptide concentration required to cause a large change in bilayer order is lower for maculatin 1.1 than for either of the two analogs due to the effect of the kink structure, which facilitates surface indentation and phospholipid disorder. In addition, the lower-temperature phase is more susceptible to peptide-induced disordering.

the peptide binding, which causes a steady drop in membrane order, indicating that below the main transition temperature, the more-rigid intermediate phase has less capacity to absorb the peptide's impact on the lipid order.

In the presence of DMPG, there was a greater propensity for the isotropic phase to exist, because the membrane was more susceptible to the disrupting effects of peptide binding, corresponding to the sharp but still reversible changes in membrane order at lower peptide levels than observed with DMPC. This reversibility was also observed for both the fluid and gel phases for each peptide, but the inflection point occurred at a higher peptide mass for the lower-temperature phase.

The influence of the Pro residue and the effect of the kink on disruption of the bilayer were clearly evident from the behavior of maculatin P15G and P15A. Maculatin P15G is more flexible than maculatin 1.1 but is likely to adopt some degree of kink structure given the flexibility of the Gly residue. Thus, when P15G approaches and binds to the membrane, the degree of indentation is less prominent and hence subsequent insertion is not as readily achievable. As a consequence, a higher amount of peptide is required to exert a disruptive effect. This effect was even more evident for P15A, which contains an Ala residue that is less flexible than Gly, is likely to adopt a relatively linear helical conformation, and is also more hydrophobic. This peptide bound more strongly than maculatin 1.1 or P15G, and the impact on bilayer structure again occurred at a higher concentration. Thus, at a given peptide concentration, the overall impact of the peptide can be evaluated in terms of the ability of the bilayer to recover from the bilayer changes induced by the binding and insertion of the peptide. Therefore, the reversibility of the changes in membrane structural integrity is a critical component of AMP action and can be measured in real time.

CONCLUSIONS

It is well accepted that cytolytic peptides act by disrupting the membrane bilayer structure in an irreversible manner. The challenge then is to understand the precise bilayer structural changes that occur before this final disruption. Such information would provide important criteria for designing peptides that can exert minor or reversible effects on mammalian cells but disrupt microbial membranes in an irreversible manner. The overall aim of this study was to investigate the role of proline in AMP structure and activity. We used solid-state NMR and DPI to obtain new (to our knowledge) insight into the structural changes in phospholipid bilayers induced by maculatin 1.1, and to provide a rationale for its generally higher potency relative to other analogs. The mode of action of AMPs can now be described in terms of the effects on membrane structure and lipid dynamics before, during, and after their interaction. Based on these studies, we propose a model for the mechanism of action for maculatin-related peptides that centers around the effect of the kinked helical structure of maculatin 1.1 on bilayer structure. The overall process is the same for the three peptides and both lipid systems, i.e., the molecular organization is essentially the same from the start of binding to the end of dissociation, but the process of going from the beginning to the end is different. The peptide kink structure facilitates the disruption after a threshold peptide level is reached, at which point the membrane integrity is either compromised or able to recover. This result has significant implications for the design of potent and selective AMPs.

SUPPORTING MATERIAL

Additional methods description, two supplemental figures, and reference (64) are available at http://www.biophysj.org/biophysj/supplemental/S0006-3495(13)00209-9.

D.I.F. received an Albert Shimmins Postgraduate Writing-Up Award from the University of Melbourne and an Australian Postgraduate Award. M.I.A. and F.S. received financial support from the Australian Research Council.

REFERENCES

1. Rozek, T., R. J. Waugh, …, J. C. Wallace. 1998. The maculatin peptides from the skin glands of the tree frog Litoria genimaculata: a comparison

of the structures and antibacterial activities of maculatin 1.1 and caerin 1.1. *J. Pept. Sci.* 4:111–115.

2. Apponyi, M. A., T. L. Pukala, …, L. E. Llewellyn. 2004. Host-defence peptides of Australian anurans: structure, mechanism of action and evolutionary significance. *Peptides.* 25:1035–1054.
3. Boland, M. P., and F. Separovic. 2006. Membrane interactions of antimicrobial peptides from Australian tree frogs. *Biochim. Biophys. Acta.* 1758:1178–1183.
4. Chia, B. C. S., J. A. Carver, …, J. H. Bowie. 2000. Maculatin 1.1, an anti-microbial peptide from the Australian tree frog, Litoria genimaculata solution structure and biological activity. *Eur. J. Biochem.* 267:1894–1908.
5. Fernandez, D. I., J. D. Gehman, and F. Separovic. 2009. Membrane interactions of antimicrobial peptides from Australian frogs. *Biochim. Biophys. Acta.* 1788:1630–1638.
6. Niidome, T., K. Kobayashi, …, H. Aoyagi. 2004. Structure-activity relationship of an antibacterial peptide, maculatin 1.1, from the skin glands of the tree frog, Litoria genimaculata. *J. Pept. Sci.* 10:414–422.
7. Brinkworth, C. S., and J. H. Bowie. 2003. Negative ion electrospray mass spectra of the maculatin peptides from the tree frogs Litoria genimaculata and Litoria eucnemis. *Rapid Commun. Mass Spectrom.* 17:2215–2225.
8. VanCompernolle, S. E., R. J. Taylor, …, D. Unutmaz. 2005. Antimicrobial peptides from amphibian skin potently inhibit human immunodeficiency virus infection and transfer of virus from dendritic cells to T cells. *J. Virol.* 79:11598–11606.
9. Seto, G. W. J., S. Marwaha, …, R. N. McElhaney. 2007. Interactions of the Australian tree frog antimicrobial peptides aurein 1.2, citropin 1.1 and maculatin 1.1 with lipid model membranes: differential scanning calorimetric and Fourier transform infrared spectroscopic studies. *Biochim. Biophys. Acta.* 1768:2787–2800.
10. Chia, C. S. B., J. Torres, …, J. H. Bowie. 2002. The orientation of the antibiotic peptide maculatin 1.1 in DMPG and DMPC lipid bilayers. Support for a pore-forming mechanism. *FEBS Lett.* 512:47–51.
11. Hall, K. N., H. Mozsolits, and M.-I. Aguilar. 2003. Surface plasmon resonance analysis of antimicrobial peptide-membrane interactions: affinity & mechanism of action. *Lett. Pept. Sci.* 10:475–485.
12. Ambroggio, E. E., F. Separovic, …, G. D. Fidelio. 2004. Surface behaviour and peptide-lipid interactions of the antibiotic peptides, Maculatin and Citropin. *Biochim. Biophys. Acta.* 1664:31–37.
13. Fernandez, D. I., M.-A. Sani, and F. Separovic. 2011. Interactions of the antimicrobial peptide maculatin 1.1 and analogues with phospholipid bilayers. *Aust. J. Chem.* 64:798–805.
14. Ambroggio, E. E., F. Separovic, …, L. A. Bagatolli. 2005. Direct visualization of membrane leakage induced by the antibiotic peptides: maculatin, citropin, and aurein. *Biophys. J.* 89:1874–1881.
15. Gehman, J. D., F. Luc, …, F. Separovic. 2008. Effect of antimicrobial peptides from Australian tree frogs on anionic phospholipid membranes. *Biochemistry.* 47:8557–8565.
16. Mechler, A., S. Praporski, …, L. L. Martin. 2007. Specific and selective peptide-membrane interactions revealed using quartz crystal microbalance. *Biophys. J.* 93:3907–3916.
17. de Kroot, A. I. P. M. 2007. Metabolism of phosphatidylcholine and its implications for lipid acyl chain composition in Saccharomyces cerevisiae. *Biochim. Biophys. Acta.* 1771:343–352.
18. Gunstone, F. D., and J. L. Harwood. 2007. Occurrence and characterisation of oils and fats. *In* The Lipid Handbook. F. D. Gunstone, J. L. Harwood, and A. J. Dijkstra, editors.. CRC Press/Taylor and Francis Group, Boca Raton, FL. 37–141.
19. Bechinger, B. 2005. Detergent-like properties of magainin antibiotic peptides: a ^{31}P solid-state NMR spectroscopy study. *Biochim. Biophys. Acta.* 1712:101–108.
20. Bechinger, B., and K. Lohner. 2006. Detergent-like actions of linear amphipathic cationic antimicrobial peptides. *Biochim. Biophys. Acta.* 1758:1529–1539.
21. Pott, T., J. Dufourcq, and E. J. Dufourcq. 1996. Fluid or gel phase lipid bilayers to study peptide-membrane interactions? *Eur. Biophys. J.* 25:55–59.
22. Dupuy, F., and R. Morero. 2011. Microcin J25 membrane interaction: selectivity toward gel phase. *Biochim. Biophys. Acta.* 1808:1764–1771.
23. Dempsey, C. E., and B. Sternberg. 1991. Reversible disc-micellization of dimyristoylphosphatidylcholine bilayers induced by melittin and [Ala-14]melittin. *Biochim. Biophys. Acta.* 1061:175–184.
24. Dufourc, E. J., I. C. P. Smith, and J. Dufourcq. 1986. Molecular details of melittin-induced lysis of phospholipid membranes as revealed by deuterium and phosphorus NMR. *Biochemistry.* 25:6448–6455.
25. Pott, T., and E. J. Dufourc. 1995. Action of melittin on the DPPC-cholesterol liquid-ordered phase: a solid state ^{2}H-and ^{31}P-NMR study. *Biophys. J.* 68:965–977.
26. Lee, T.-H., C. Heng, …, M. I. Aguilar. 2010. Real-time quantitative analysis of lipid disordering by aurein 1.2 during membrane adsorption, destabilisation and lysis. *Biochim. Biophys. Acta.* 1798:1977–1986.
27. Balla, M. S., J. H. Bowie, and F. Separovic. 2004. Solid-state NMR study of antimicrobial peptides from Australian frogs in phospholipid membranes. *Eur. Biophys. J.* 33:109–116.
28. Fernandez, D. I., M.-A. Sani, …, F. Separovic. 2011. Interactions of a synthetic Leu-Lys-rich antimicrobial peptide with phospholipid bilayers. *Eur. Biophys. J.* 40:471–480.
29. Lam, Y.-H., S. R. Wassall, …, F. Separovic. 2001. Solid-state NMR structure determination of melittin in a lipid environment. *Biophys. J.* 81:2752–2761.
30. Sani, M.-A., F. Separovic, and J. D. Gehman. 2011. Disentanglement of heterogeneous dynamics in mixed lipid systems. *Biophys. J.* 100: L40–L42.
31. Sherman, P. J., R. J. Jackway, …, J. H. Bowie. 2009. Solution structure and membrane interactions of the antimicrobial peptide fallaxidin 4.1a: an NMR and QCM study. *Biochemistry.* 48:11892–11901.
32. Smith, R., F. Separovic, …, B. A. Cornell. 1992. Melittin-induced changes in lipid multilayers. A solid-state NMR study. *Biophys. J.* 63:469–474.
33. Fernandez, D. I., A. P. L. Brun, …, F. Separovic. 2012. Structural effects of the antimicrobial peptide maculatin 1.1 on supported lipid bilayers. *Eur. Biophys. J.* 42:47–59.
34. Lee, T.-H., and M.-I. Aguilar. 2011. Dual polarization interferometry: an optical biosensor which allows new insights into peptide-induced changes in biomembrane structure. *Aust. J. Chem.* 64:844–845.
35. Lee, T.-H., K. N. Hall, …, M. I. Aguilar. 2010. The membrane insertion of helical antimicrobial peptides from the N-terminus of Helicobacter pylori ribosomal protein L1. *Biochim. Biophys. Acta.* 1798:544–557.
36. Ambroggio, E. E., M. A. Villarreal, …, G. D. Fidelio. 2006. Interfacial properties of the M1 segment of the nicotinic acetylcholine receptor. *Biophys. Chem.* 121:171–176.
37. de Planque, M. R. R., D. T. S. Rijkers, …, F. Separovic. 2004. The alphaM1 segment of the nicotinic acetylcholine receptor exhibits conformational flexibility in a membrane environment. *Biochim. Biophys. Acta.* 1665:40–47.
38. Ho, B. K., E. A. Coutsias, …, K. A. Dill. 2005. The flexibility in the proline ring couples to the protein backbone. *Protein Sci.* 14:1011–1018.
39. Kim, C., T. Schmidt, …, M. H. Ginsberg. 2012. Basic amino-acid side chains regulate transmembrane integrin signalling. *Nature.* 481: 209–213.
40. Matsushima, N., H. Yoshida, …, R. H. Kretsinger. 2008. Flexible structures and ligand interactions of tandem repeats consisting of proline, glycine, asparagine, serine, and/or threonine rich oligopeptides in proteins. *Curr. Protein Pept. Sci.* 9:591–610.
41. Porcelli, F., B. Buck, …, G. Veglia. 2004. Structure and orientation of pardaxin determined by NMR experiments in model membranes. *J. Biol. Chem.* 279:45815–45823.

42. Sani, M.-A., C. Loudet, …, E. J. Dufourc. 2007. Pro-apoptotic bax-α1 synthesis and evidence for β-sheet to α-helix conformational change as triggered by negatively charged lipid membranes. *J. Pept. Sci.* 13: 100–106.

43. Davis, J. H., M. Bloom, …, I. C. Smith. 1980. The temperature dependence of molecular order and the influence of cholesterol in *Acholeplasma laidlawii* membranes. *Biochim. Biophys. Acta.* 597:477–491.

44. Cho, N.-J., C. W. Frank, …, F. Höök. 2010. Quartz crystal microbalance with dissipation monitoring of supported lipid bilayers on various substrates. *Nat. Protoc.* 5:1096–1106.

45. Richter, R. P., R. Bérat, and A. R. Brisson. 2006. Formation of solid-supported lipid bilayers: an integrated view. *Langmuir.* 22:3497–3505.

46. Castellana, E. T., and P. S. Cremer. 2006. Solid supported lipid bilayers: from biophysical studies to sensor design. *Surf. Sci. Rep.* 61:429–444.

47. Hirst, D. J., T.-H. Lee, …, M. I. Aguilar. 2011. Effect of acyl chain structure and bilayer phase state on binding and penetration of a supported lipid bilayer by HPA3. *Eur. Biophys. J.* 40:503–514.

48. Cross, G. H., A. Reeves, …, J. R. Lu. 2004. The metrics of surface adsorbed small molecules on the Young's fring dual-slab waveguide interferometer. *J. Phys. D Appl. Phys.* 37:74–80.

49. Mashaghi, A., M. Swann, …, E. Reimhult. 2008. Optical anisotropy of supported lipid structures probed by waveguide spectroscopy and its application to study of supported lipid bilayer formation kinetics. *Anal. Chem.* 80:3666–3676.

50. Swann, M. J., L. L. Peel, …, N. J. Freeman. 2004. Dual-polarization interferometry: an analytical technique to measure changes in protein structure in real time, to determine the stoichiometry of binding events, and to differentiate between specific and nonspecific interactions. *Anal. Biochem.* 329:190–198.

51. Seelig, J., and W. Niederberger. 1974. Deuterium-labelled lipids as structural probes in liquid crystalline bilayers: a deuterium magnetic resonance study. *J. Am. Chem. Soc.* 96:2069–2072.

52. Cullis, P. R., and B. de Kruijff. 1979. Lipid polymorphism and the functional roles of lipids in biological membranes. *Biochim. Biophys. Acta.* 559:399–420.

53. Seelig, J. 1978. ^{31}P nuclear magnetic resonance and the headgroup structure of phospholipids in membranes. *Biochim. Biophys. Acta.* 515:105–140.

54. Silvius, J. R. 1982. Thermotropic phase transitions of pure lipids in model membranes and their modifications by membrane proteins. *In* Lipid-Protein Interactions.. John Wiley & Sons, New York.

55. Kranenburg, M., and B. Smit. 2005. Phase behavior of model lipid bilayers. *J. Phys. Chem. B.* 109:6553–6563.

56. Nagle, J. F., and S. Tristram-Nagle. 2000. Structure of lipid bilayers. *Biochim. Biophys. Acta.* 1469:159–195.

57. Epand, R. F., W. L. Maloy, …, R. M. Epand. 2010. Probing the "charge cluster mechanism" in amphipathic helical cationic antimicrobial peptides. *Biochemistry.* 49:4076–4084.

58. Epand, R. F., L. Maloy, …, R. M. Epand. 2010. Amphipathic helical cationic antimicrobial peptides promote rapid formation of crystalline states in the presence of phosphatidylglycerol: lipid clustering in anionic membranes. *Biophys. J.* 98:2564–2573.

59. Shai, Y. 2002. Mode of action of membrane active antimicrobial peptides. *Biopolymers.* 66:236–248.

60. Shai, Y. 1999. Mechanism of the binding, insertion and destabilization of phospholipid bilayer membranes by α-helical antimicrobial and cell non-selective membrane-lytic peptides. *Biochim. Biophys. Acta.* 1462:55–70.

61. Ahyayauch, H., M. I. Collado, …, F. M. Goñi. 2012. Lipid bilayers in the gel phase become saturated by triton X-100 at lower surfactant concentrations than those in the fluid phase. *Biophys. J.* 102:2510–2516.

62. Vermeer, L. S., Y. Lan, …, A. J. Mason. 2012. Conformational flexibility determines selectivity and antibacterial, antiplasmodial, and anticancer potency of cationic α-helical peptides. *J. Biol. Chem.* 287:34120–34133.

63. Yang, L., T. A. Harroun, …, H. W. Huang. 2001. Barrel-stave model or toroidal model? A case study on melittin pores. *Biophys. J.* 81:1475–1485.

64. De Feijter, J. A., J. Benjamins, and F. A. Veer. 1978. Ellipsometry as a tool to study the adsorption behavior of synthetic and biopolymers at the air-water interface. *Biopolymers.* 17:1759–1772.